DOI: 10.1002/((please add manuscript number))
Article type: Communication

Fabrication and Operating Mechanism of Deep-UV Transparent Semiconducting $SrSnO_3$-based Thin Film Transistor

Mian Wei, Lizhikun Gong, Dou-dou Liang, Hai Jun Cho, and Hiromichi Ohta**

M. Wei, L. Gong, Prof. H.J. Cho, Prof. H. Ohta
Graduate School of Information Science and Technology, Hokkaido University, N14W9, Kita, Sapporo 060−0814, Japan

D. Liang
The Beijing Municipal Key Laboratory of New Energy Materials and Technologies, School of Materials Science and Engineering, University of Science and Technology Beijing, Beijing 100083, China

D. Liang, Prof. H.J. Cho, Prof. H. Ohta
Research Institute for Electronic Science, Hokkaido University, N20W10, Kita, Sapporo 001−0020, Japan
E-mail: joon@es.hokudai.ac.jp, hiromichi.ohta@es.hokudai.ac.jp

Keywords: deep-UV transparent semiconductor, $SrSnO_3$, thermopower modulation, effective thickness

Thin film transistor (TFT) with deep-UV transparency is a promising component for the next generation optoelectronics such as biosensor. Among several deep-UV transparent oxide semiconductors, $SrSnO_3$ is an excellent candidate material owing to its wide bandgap (~4.6 eV) and rather high carrier electron mobility. Here we show fabrication and operation mechanism of the $SrSnO_3$-TFT. We fabricated metal-insulator-semiconductor structure on the 28-nm-thick $SrSnO_3$ film. The resultant TFT showed clear transistor characteristics; the on-to-off current ratio was ~10^2, the threshold voltage was ~ −18 V, and the field effect mobility was ~14 $cm^2 V^{-1} s^{-1}$. The effective thickness of the electron channel gradually increased with gate voltage and saturated at ~5 nm, which was evaluated by the thermopower modulation. The present results would be helpful for utilizing deep-UV transparent TFTs for biosensing applications.

Deep-UV (DUV, 200−300 nm in wavelength) transparent oxide semiconductors (TOSs)[1, 2] with high carrier mobility are promising candidates as the active layer of thin-film transistors (TFTs) for next generation optoelectronics such as biosensors[3, 4] and biotransistors[5]. For instance, DNA and proteins have characteristic absorption and/or fluorescence in DUV region. Very recently, Zhang and Amano *et al*. demonstrated room temperature operation of deep-UV laser diode (271.8 nm),[6] which can be used for ultra-large-scale integrated lithography and higher density optical memories. Zheng *et al*. developed vacuum UV detectors utilizing the photovoltaic effect of Graphene/AlN/p-type GaN on vacuum UV light (10−200 nm).[7] With the realization of high-quality DUV transparent TFTs, efficient DUV optoelectronic device performance can be realized. In this regard, electric field modulation in metal-insulator-semiconductor (MIS) configuration is ideal since it allows large gain and high sensitivity in tracing the accumulated charges in the channel, which has a great potential in sensing applications.

For the active layer in the DUV-transparent TFT, there are several DUV-TOS candidates such as β-Ga_2O_3 (E_g ~4.9 eV, ~1 S cm^{-1})[8, 9], α-Ga_2O_3 (E_g ~5.3 eV, ~0.3 S cm^{-1})[10], electron-doped calcium aluminate (C12A7:e^-, ~4 eV, ~800 S cm^{-1})[11-13]. However, the TFT based on these materials exhibit poor performances, probably due to the relatively low electron mobility. For instance, the mobility of Ga_2O_3 based TFT shows only 5×10^{-2} cm^2 V s^{-1} with current on/off ratio of ~20.[14] The performance of DUV transparent TFT can potentially be improved using $SrSnO_3$, which has a very large bandgap (~4.6 eV[15, 16]) as well as sufficient thin film mobility (~56 cm^2 V^{-1} s^{-1}) and electrical conductivity (σ = 3000 S cm^{-1}) at significantly high carrier concentrations (3.26×10^{20} cm^{-3}).[17, 18] For these reasons, examining electric field-induced properties of active $SrSnO_3$ channel of the TFT is of great importance.

There are a few papers reporting $SrSnO_3$-based TFTs. In 2018, Chaganti *et al.*[19] reported a depletion-mode $SrSnO_3$ n-channel metal-semiconductor FET (MESFET). In 2019, Thoutam *et al.*[20] reported the ion gel gating of La-doped $SrSnO_3$ films grown by MBE, where they successfully modulated the conductivity using the large capacitance of ion gel. However, $SrSnO_3$ TFTs with the MIS configuration has not been realized to date. Recently, we clarified the operation mechanism of MIS-TFTs using $Ba_{1-x}Sr_xSnO_3$ solid solution as the active layers and found that the effective thickness t_{eff} ($\equiv n_{2D}/n_{3D}$) of the conducting channel goes up with increasing x, whereas the carrier effective mass m^* becomes lighter. The former is attributed to the increase in E_g while the latter is due to the overlap enhancements of neighboring Sn 5s orbitals.[21] The increase in E_g suppressed the formation of electron channels, which eventually prevented the undoped $SrSnO_3$ based TFT from functioning properly. In order to overcome this difficulty, we used slightly La-doped $SrSnO_3$ as the channel material since doping can bring the Fermi level closer to the bottom of the conduction band, enabling the TFT behaviors.

Here we demonstrate the fabrication and characterization of functioning $SrSnO_3$-TFT with MIS configuration. The resultant TFT showed the on-to-off current ratio of ~10^2, the threshold voltage of ~ −18 V, and the field effect mobility of ~14 $cm^2\ V^{-1}\ s^{-1}$. We also clarified that the effective thickness of the TFT channel gradually increased with gate voltage and saturated at ~5 nm. The present results are the pioneering steps for utilizing deep-UV transparent TFTs for biosensor applications.

We fabricated top-gate type TFTs (**Figure 1a**) on a 5% La-doped $SrSnO_3$ film, which was grown on a (001)-oriented $SrTiO_3$ single crystal substrate (1 cm × 1 cm × 0.5 mm) using pulsed laser deposition (PLD) technique followed by thermal annealing at 1200 °C in air to obtain atomically flat surface.[21-23] Before the TFT fabrication, we analyzed the

crystallographic features of the La-doped $SrSnO_3$ film using high resolution X-ray diffraction (XRD) and atomic force microscopy (AFM). Kiessig fringes were clearly observed in the X-ray reflectivity (**Figure 1b**), indicating the top surface and the interface between the film and the substrate are atomically flat. From the fringes, the film thickness of La-doped $SrSnO_3$ film was calculated to be 28 nm. No peaks other than the intense diffraction peaks of 00*l* La-doped $SrSnO_3$ film and 00*l* $SrTiO_3$ substrate were observed in the out-of-plane XRD pattern (**Figure 1c**). Pendellösung fringes were clearly observed around 00*l* La-doped $SrSnO_3$ (the inset of **Figure 1c**), indicating strong 00*l* crystallographic texture of the film. The full-width-at-half-maximum (FWHM) of the out-of-plane X-ray rocking curve of the 002 La-doped $SrSnO_3$ film was 0.02° (**Figure 1d**), which corresponds to the resolution of the diffractometer with two crystals of Ge monochrometer. Atomically smooth surface with stepped and terraced structure was confirmed in the topographic AFM image of the La-doped $SrSnO_3$ film (**Figure 1e**). These results indicate the excellent crystal quality of the La-doped $SrSnO_3$ film.

After the deposition of La-doped $SrSnO_3$ channel, we deposited 30-nm-thick metallic Ti for the source and drain electrodes through stencil masks using the electron beam (EB) evaporation technique. Then, ~300-nm-thick amorphous $12CaO{\cdot}7Al_2O_3$ (a-C12A7, the dielectric permittivity, $\varepsilon_r = 12$)[24, 25] film was deposited by PLD at room temperature as the gate insulator. Finally, we deposited 20-nm-thick metallic Ti film for the gate electrode. The channel width *W* and channel length *L* were 400 μm and 800 μm, respectively. The TFT was put between two Peltier devices separated by ~2-mm to introduce a temperature difference to the channel. K-type thermocouples (K-T.C.) were used to measure the temperature difference between the source and the drain. The details of our experimental setup are described in the **Experimental Section**.

The transistor characteristics of the resultant TFTs were measured by a semiconductor device analyzer (B1500A, Agilent) at room temperature in a shield box. As shown in **Figure 2a**, the resultant TFTs showed clear transistor characteristics with the on-to-off current ratio of ~10^2. A threshold gate voltage of ~−18 V was evaluated by plotting $I_d^{0.5}$–V_g relationship (**Figure S1a**). The TFT shows clear pinch-off behavior in the output characteristics (**Figure 2b**), which is a standard behavior of field-effect transistors. The field effect mobility (μ_{FE}), calculated from $\mu_{FE} = g_m \cdot [(W/L) \cdot C_i \cdot V_d]^{-1}$, where g_m is the transconductance $\partial I_d/\partial V_g$ and C_i is capacitance per unit area (C_i ~35.3 nF cm^{-2}), was ~14 cm^2 V^{-1} s^{-1} at the gate voltage of +7 V (**Figure S1b**). The electric field modulated thermopower (S) was measured during the transfer characteristics measurements to analyze the t_{eff} of the conducting channel. The S values were negative, consistent with the fact that La-doped $SrSnO_3$ films are n-type semiconductors. **Figure 2c** shows changes in the $-S$ as a function of the gate voltage (V_g). The absolute values of S gradually decrease with increasing V_g.

We then plotted the electric field modulated S as a function of the sheet carrier concentration (n_s), which is calculated from $n_s = C_i \cdot (V_g - V_{th}) \cdot e^{-1}$ (**Figure 3a**). The $-S$ decreases linearly at ~ –160 μV K^{-1} decade^{-1} with increasing n_s in a logalithmic scale. Since the t_{eff} of the TFT channel can be estimated as n_s/n_v, where n_v is volume carrier concentration, we also measured the S of La-doped $SrSnO_3$ ($La_xSr_{1-x}SnO_3$, x = 0.02, 0.03, and 0.05) films as a functions of carrier concerntration. Using the dopant controlled La-doped $SrSnO_3$ films, we plotted the volume carrier concentration (n_v) dependence of $-S$ for the La-doped $SrSnO_3$ thin films (**Figure 3b**, **Table S1**). From these $-S$ vs. n_v relationship, the m^* of the La-doped $SrSnO_3$ films was extracted to be 0.23 m_e using the following equations.

$$n_{-} = 4\pi \left(\frac{2m^* k_B T}{h^2} \right)^{3/2} F_{1/2}(\xi) \qquad (1)$$

$$F_r(\xi) = \int_0^\infty \frac{x^r}{1+e^{x-\xi}} dx \qquad (2)$$

$$S = -\frac{k_B}{e}\left(\frac{(r+2)F_{r+1}(\xi)}{(r+1)F_r(\xi)} - \xi\right) \qquad (3)$$

where k_B, T, h, ξ, r, and F_r are the Boltzmann constant, absolute temperature, the Planck constant, reduced Fermi energy, scattering parameter of relaxation time, and Fermi integral, respectively. We assumed the r value of 0.5 (optical phonon scattering) because the temperature dependence of Hall mobility showed that optical phonon scattering is dominant at room temperature (data not shown). Then we calculated full range $-S$ vs. n_v relationship (dotted line).

In **Figure 3**, we compare the $-S$ vs. n_s relationship with the $-S$ vs. n_v relationship. Since the slope of $-S$ vs. logarithmic n_v is comparable to that of $-S$ vs. logarithmic n_s (–160 μV K^{-1} $decade^{-1}$), the t_{eff} can be extracted as n_s/n_v, which is plotted in **Figure 3c** as a function of V_g. The t_{eff} of the conducting La-doped $SrSnO_3$ channel increases with V_g and saturates around 5 nm. From these results, we can simply analyze the operation mechanism of the $SrSnO_3$-based TFT. As a degenerate semiconductor, the conduction electrons (blue points, **Figure 4a**) are located at the conduction band minimum (CBM) without any V_g application. Under small positive V_g application (**Figure 4b**), a two-dimensional electron gas (2DEG) layer is formed at the heterointerface. The thickness of this 2DEG channel t_{eff} gradually increases with increasing V_g, and saturated at ~5 nm as described above (**Figure 4c**).

Finally, we measured the optical transmission and reflection spectra of the multilayer of a-C12A7 film (300 nm) / La-doped $SrSnO_3$ film (23 nm) grown on a (001) MgO substrate (0.5 mm) (**Figure S2**). Since most DNA show their absorption peaking around 260 nm in wavelength, high transparency at 260 nm is required to develop a biotransistor. The optical

transmission at 260 nm in wavelength is greater than 50%, suggesting that the present DUV transparent TFT would be suitable as a biotransistor. For example, biosensing can be possible simultaneously with observing the images by transmission optical microscopy under the DUV photoexcitation of DNA. This is a great advantage of the DUV transparent TFT because conventional Si-based TFT cannot be applied for this purpose. We will investigate the feasibility of the DUV transparent TFT based biotransistor composed of La-doped $SrSnO_3$ thin film near future.

In summary, we successfully fabricated La-doped $SrSnO_3$-based TFT with MIS configuration, which show a field effect mobility of ~14 $cm^2\ V^{-1}\ s^{-1}$ at a gate voltage of +7 V. The on-to-off current ratio was ~10^2. The threshold voltage was −18 V, and the output characteristic curves showed pinch-off behavior. We also showed the operation mechanism of the resultant TFT. By combing the electric field modulation method with the n_v dependences of S, we clarified that the effective thickness of the conducting channel of TFT. The effective thickness was gradually increased with gate voltage and saturated at ~5 nm. These results are an important step toward the realization of biosensors utilizing deep-UV transparent TFTs.

Experimental Section

Growth and Analyses of the La-doped $SrSnO_3$ epitaxial film: 5%-La-doped $SrSnO_3$ epitaxial film was fabricated on (001) $SrTiO_3$ (cubic, a = 0.3905 nm) single crystal substrates by pulsed laser deposition (PLD) technique (KrF excimer laser, λ = 248 nm, fluence ~2 J cm^{-2} $pulse^{-1}$, repetition rate = 10 Hz) using $La_{0.05}Sr_{0.95}SnO_3$ ceramic as the target material. During the film growth, substrate temperature and oxygen pressure inside the chamber were kept at 750 °C and 20 Pa, respectively. After the film growth, we turned off the substrate heater immediately and cooled the sample down to room temperature. The crystalline phase, orientation, lattice

parameters, and thickness of the films were analyzed by high-resolution X-ray diffraction (Cu $K\alpha_1$, ATX-G, Rigaku Co.). Out-of-plane Bragg diffraction patterns and the rocking curves were measured at room temperature. X-ray reflection patterns were measured to evaluate the density and the thickness. An atomic force microscopy (AFM, Nanocute, Hitachi Hi-Tech Sci. Co.) was used to observe the surface microstructure of the films. In addition, several $La_xSr_{1-x}SnO_3$ (x = 0.05, 0.03 and 0.02) epitaxial thin films were also fabricated on (001) $SrTiO_3$ substrates.

Fabrication of the TFT: The three-terminal TFT structures were fabricated on 28-nm-thick 5%-La-doped $SrSnO_3$ film grown on (001) $SrTiO_3$ single crystal substrate. Frist, 30-nm-thick metallic Ti films for the source and drain electrodes were deposited on the La-doped $SrSnO_3$ film surface using the electron beam (EB) evaporation through the stencil mask at room temperature. Then, around 300-nm-thick amorphous $12CaO{\cdot}7Al_2O_3$ (a-C12A7, the dielectric permittivity, ε_r = 12)[24] was deposited by PLD under 0.1 Pa oxygen atmosphere at room temperature. After that, 20-nm-thick Ti film for the gate electrode was deposited on the a-C12A7 film by the EB evaporation through the stencil mask at room temperature. The channel width W and channel length L were 400 μm and 800 μm, respectively. The resultant TFT device was annealed at 150 °C in air for 30 min, mainly to remove the residual water in C12A7, thereby reducing the leakage current.

Transistor Characteristics and Thermopower Measurements of the TFT: The transfer characteristics (I_d–V_g) and the output characteristics (I_d–V_d) were measured using a semiconductor device analyzer (B1500A, Agilent Co.) at room temperature in air. The capacitance of the gate insulator was measured using LCR meter. Thermopower (S) of the TFT channel was measured by the electric filed S modulation method. The TFT device was placed on the gap (~2 mm) between two Peltier devices, which were used to generate a

temperature difference between the source and the drain electrodes. One Peltier device was used as the heater and the other one was used as the cooler, when the electric current is applied to the Peltier devices simultaneously. Two tiny thermocouples (K-type), which were mechanically attached at both edges of the La-doped $SrSnO_3$ channel, were used to monitor the temperature difference (ΔT, 0–1 K). The thermo-electromotive force (ΔV) and ΔT values were simultaneously measured at room temperature, and the slope of the ΔV–ΔT plots yielded the *S*-values. Details of our electric field modulated *S* measurement are described elsewhere.[21, 23-29]

Supporting Information
Supporting Information is available from the Wiley Online Library or from the author.

Acknowledgements
This research was supported by Grants-in-Aid for Scientific Research A (17H01314) and Innovative Areas (19H05791) from the JSPS. A part of this work was supported by Dynamic Alliance for Open Innovation Bridging Human, Environment, and Materials, and by the Network Joint Research Center for Materials and Devices. H.J.C. acknowledges the support from Nippon Sheet Glass Foundation for Materials Science and Engineering. H.O. acknowledges the support from the Asahi Glass Foundation and the Mitsubishi Foundation The support from China Scholarships Council (M. Wei: 201808050081, D. Liang: 201806460051) is also greatly appreciated. M. Wei, D. Liang, and L. Gong contributed equally to this work.

Conflict of Interest
The authors declare no conflict of interest.

Received: ((will be filled in by the editorial staff))
Revised: ((will be filled in by the editorial staff))
Published online: ((will be filled in by the editorial staff))

References

[1] D. Ginley, H. Hosono, D. C. Paine, in *Handbook of Transparent Conductors*, 2011th Edition ed., Springer, **2011**.

[2] H. Hosono, *Thin Solid Films* **2007**, *515*, 6000-6014.

[3] J. Kim, A. S. Campbell, B. E. F. de Avila, J. Wang, *Nat. Biotechnol.* **2019**, *37*, 389-406.

[4] Y. R. Yang, W. Gao, *Chem. Soc. Rev.* **2019**, *48*, 1465-1491.

[5] S. N. Kim, J. F. Rusling, F. Papadimitrakopoulos, *Adv. Mater.* **2007**, *19*, 3214-3228.

[6] Z. Zhang, M. Kushimoto, T. Sakai, N. Sugiyama, L. J. Schowalter, C. Sasaoka, H. Amono, *Appl. Phys. Express* **2019**, *12*, 124003.

[7] W. Zheng, R. C. Lin, J. X. Ran, Z. J. Zhang, X. Ji, F. Huang, *ACS Nano* **2018**, *12*, 425-431.

[8] M. Orita, H. Ohta, M. Hirano, H. Hosono, *Appl. Phys. Lett.* **2000**, *77*, 4166-4168.

[9] R. Wakabayashi, K. Yoshimatsu, M. Hattori, A. Ohtomo, *Appl. Phys. Lett.* **2017**, *111*, 162101.

[10] H. Ito, K. Kaneko, S. Fujita, *Jpn. J. Appl. Phys.* **2012**, *51*, 100207.

[11] M. Miyakawa, K. Hayashi, M. Hirano, Y. Toda, T. Kamiya, H. Hosono, *Adv. Mater.* **2003**, *15*, 1100-1103.

[12] S. Matsuishi, Y. Toda, M. Miyakawa, K. Hayashi, T. Kamiya, M. Hirano, I. Tanaka, H. Hosono, *Science* **2003**, *301*, 626-629.

[13] K. Hayashi, S. Matsuishi, T. Kamiya, M. Hirano, H. Hosono, *Nature* **2002**, *419*, 462-465.

[14] K. Matsuzaki, H. Yanagi, T. Kamiya, H. Hiramatsu, K. Nomura, M. Hirano, H. Hosono, *Appl. Phys. Lett.* **2006**, *88*, 092106.

[15] H. Mizoguchi, H. W. Eng, P. M. Woodward, *Inorg. Chem.* **2004**, *43*, 1667-1680.

[16] D. J. Singh, Q. Xu, K. P. Ong, *Appl. Phys. Lett.* **2014**, *104*, 011910.

[17] T. Q. Wang, L. R. Thoutam, A. Prakash, W. Nunn, G. Haugstad, B. Jalan, *Phys. Rev. Mater.* **2017**, *1*, 061601(R).

[18] M. Wei, A. V. Sanchela, B. Feng, Y. Ikuhara, H. J. Cho, H. Ohta, *Appl. Phys. Lett.* **2020**, *116*, 022103.

[19] V. R. S. K. Chaganti, A. Prakash, J. Yue, B. Jalan, S. J. Koester, *IEEE Electron Device Lett.* **2018**, *39*, 1381-1384.

[20] L. R. Thoutam, J. Yue, A. Prakash, T. Q. Wang, K. E. Elangovan, B. Jalan, *ACS Appl. Mater. Interfaces* **2019**, *11*, 7666-7670.

[21] A. V. Sanchela, M. Wei, H. J. Cho, H. Ohta, *Small* **2019**, *15*, 1805394.

[22] J. Shiogai, K. Nishihara, K. Sato, A. Tsukazaki, *AIP Adv.* **2016**, *6*, 065305.

[23] A. V. Sanchela, T. Onozato, B. Feng, Y. Ikuhara, H. Ohta, *Phys. Rev. Materials* **2017**, *1*, 034603.

[24] H. Ohta, Y. Sato, T. Kato, S. Kim, K. Nomura, Y. Ikuhara, H. Hosono, *Nature Commun.* **2010**, *1*, 118.

[25] H. Ohta, Y. Masuoka, R. Asahi, T. Kato, Y. Ikuhara, K. Nomura, H. Hosono, *Appl. Phys. Lett.* **2009**, *95*, 113505.

[26] H. Ohta, S. W. Kim, S. Kaneki, A. Yamamoto, T. Hashizume, *Adv. Sci.* **2018**, *5*, 1700696.

[27] T. Mizuno, Y. Nagao, A. Yoshikawa, K. Koumoto, T. Kato, Y. Ikuhara, H. Ohta, *J. Appl. Phys.* **2011**, *110*, 063719.

[28] Y. Nagao, A. Yoshikawa, K. Koumoto, T. Kato, Y. Ikuhara, H. Ohta, *Appl. Phys. Lett.* **2010**, *97*, 172112.

[29] H. Koide, Y. Nagao, K. Koumoto, Y. Takasaki, T. Umemura, T. Kato, Y. Ikuhara, H. Ohta, *Appl. Phys. Lett.* **2010**, *97*, 182105.

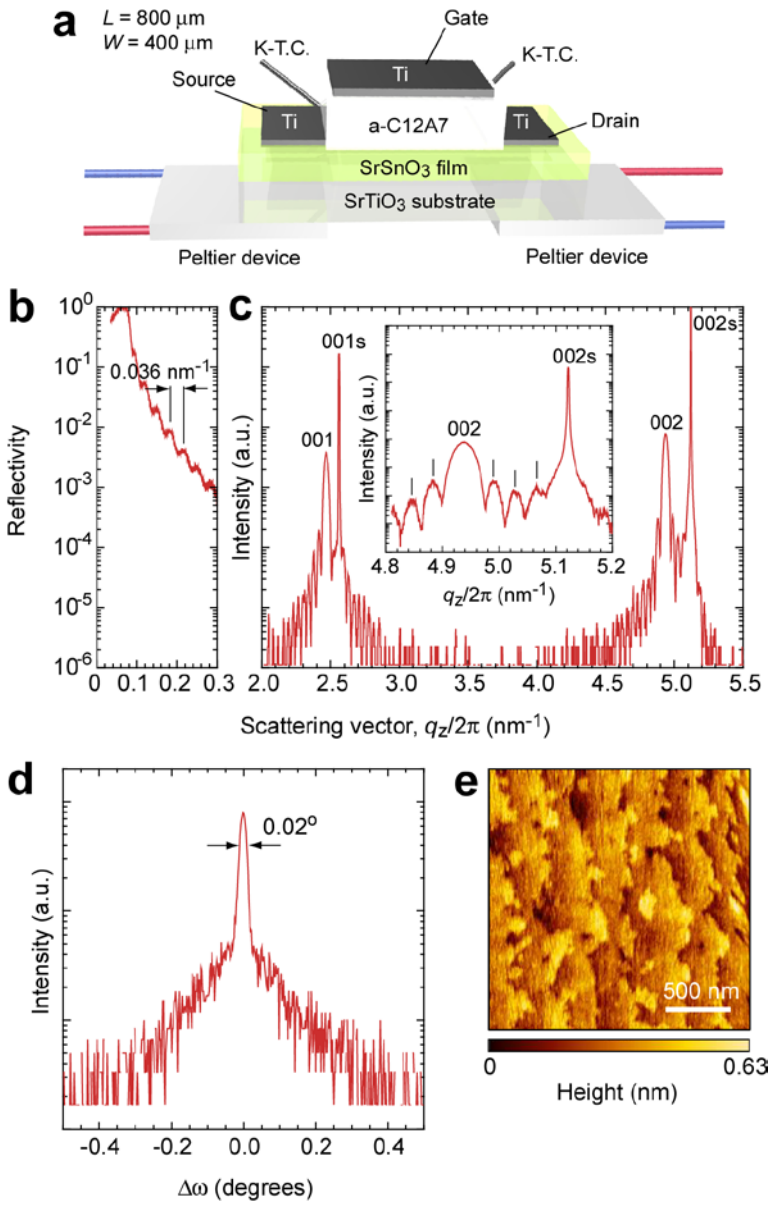

Figure 1. La-doped $SrSnO_3$-based TFT. (a) Schematic illustration of the La-doped $SrSnO_3$-based TFT, which is placed on the gap between two Peltier devices. The Peltier devices are used to provide temperature difference (ΔT) between both edges of the TFT channel. The thermo-electromotive force (ΔV) and ΔT are measured simultaneously during gate voltage (V_g) application. (b) X-ray reflection pattern of the La-doped $SrSnO_3$ film. Kiessig fringes observed at lower scattering vector were used to calculate the thickness of the La-doped $SrSnO_3$ films, which was 27.8 nm. (c) Out-of-plane XRD pattern. The inset is the zoomed region around the 002 Bragg peak of La-doped $SrSnO_3$. Pendellösung fringes are clearly observed around 00*l* diffraction peaks. (d) Rocking curve of the 002 La-doped $SrSnO_3$. The full-width-at-half-maximum (FWHM) is 0.02°, showing strong 00*l* orientation of the film. (e) Topographic AFM image of the La-doped $SrSnO_3$ film. Stepped and terraced surface is seen.

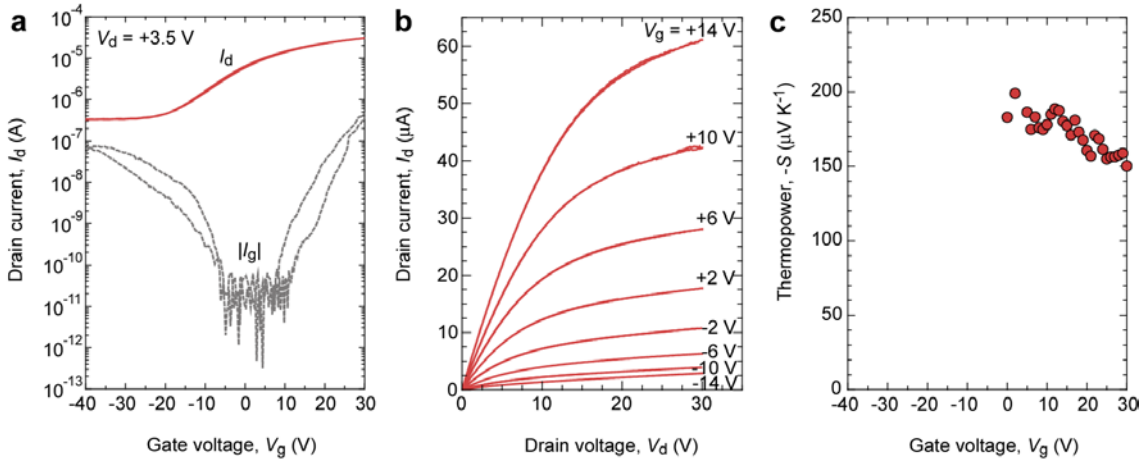

Figure 2. Transistor characteristics of the resultant TFT at room temperature. (a) Transfer (I_d−V_g) characteristics (V_d = 3.5 V). The absolute values of the gate leakage current ($|I_g|$) are also plotted. The on-to-off current ratio of I_d is ~10^2. (b) Output characteristics. Pinch-off behavior is clearly seen. (c) Change in the thermopower (S) as a function of V_g. The −S gradually decreases with V_g.

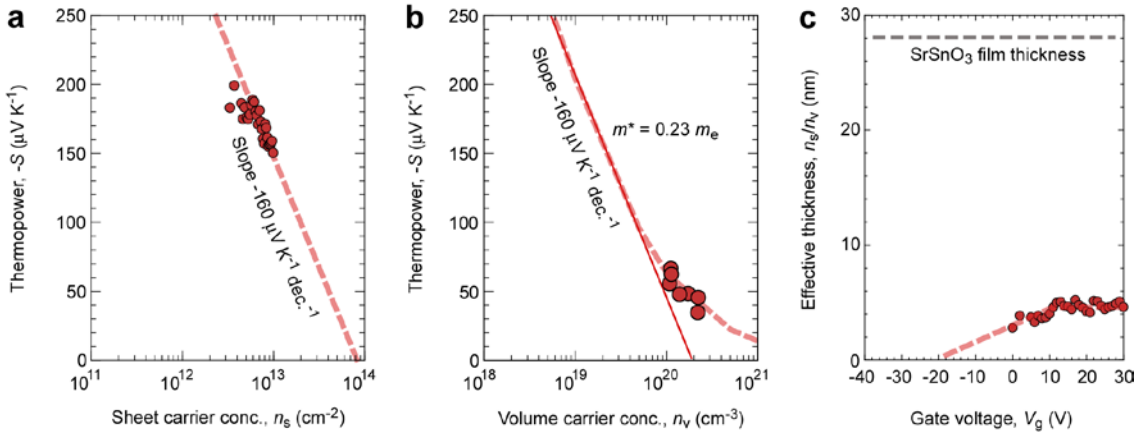

Figure 3. Electric field thermopower modulation analysis of the $SrSnO_3$-based TFT at room temperature. (a) Sheet carrier concentration (n_s) dependences of S. The slope of S–n_s relationship is −160 μV K^{-1} $decade^{-1}$ (dotted line). (b) Volume carrier concentration (n_v) dependence S of the La-doped $SrSnO_3$ films. We calculated the carrier effective mass (m^*) of the La-doped $SrSnO_3$ film around 0.23 m_e. The dotted line indicates the result of the calculation of S. A linear line can be drawn with a slope of −160 μV K^{-1} $decade^{-1}$. (c) The effective thickness (t_{eff}), which is defined as n_s/n_v, as a function of V_g. The t_{eff} increases with V_g and saturates around 5 nm, whereas the La-doped $SrSnO_3$ film thickness is 28 nm.

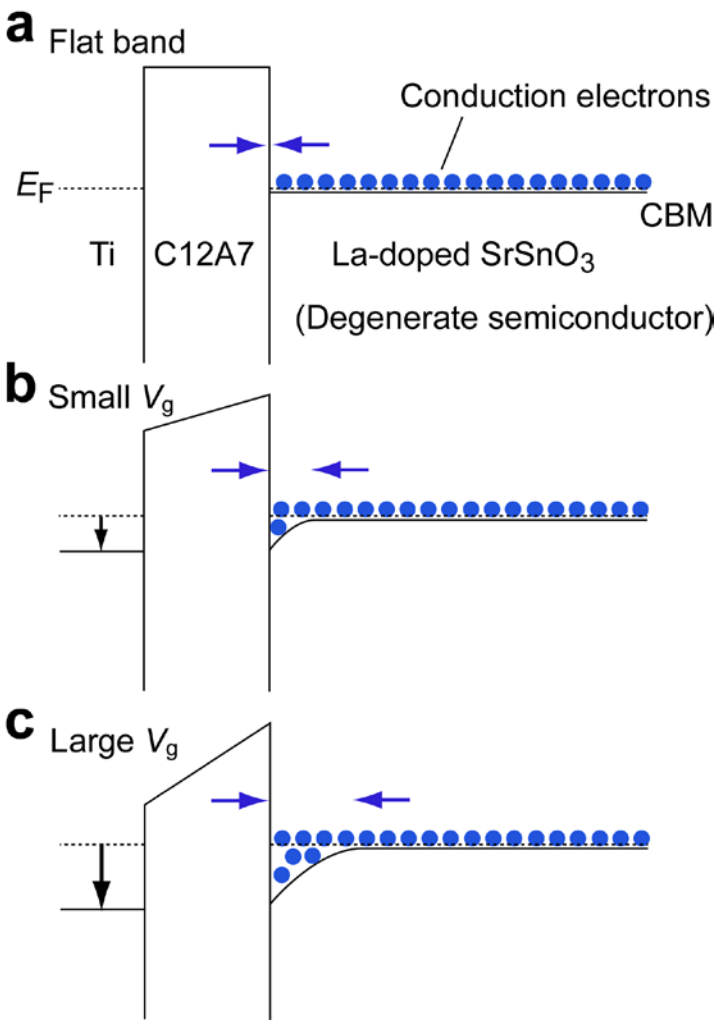

Figure 4. Electric field modulation mechanism of the $SrSnO_3$-based TFT. (a) Without any gate voltage (V_g) application. (b) Under small V_g application. The conduction band bending happened. The conducting channel formed at the C12A7/La-doped $SrSnO_3$ interface. The thickness of conducting channel (t_{eff}) gradually increases up to ~5 nm. (c) Under large V_g application. The t_{eff} saturated at ~5 nm.

Deep-ultraviolet (DUV, 200−300 nm in wavelength) transparent oxide semiconductor, $SrSnO_3$-based thin film transistor (TFT) was realized. The resultant transistor showed clear transistor characteristics and the effective thickness of the conducting channel was clarified by the electric field thermopower modulation measurements. The present results are the pioneering steps for utilizing DUV transparent TFTs for biosensor applications.

Keyword deep-UV transparent semiconductor, $SrSnO_3$, thermopower modulation, effective thickness

M. Wei, L. Gong, D. Liang, H.J. Cho*, H. Ohta*

Fabrication and Operating Mechanism of Deep-UV Transparent Semiconducting $SrSnO_3$-based Thin Film Transistor

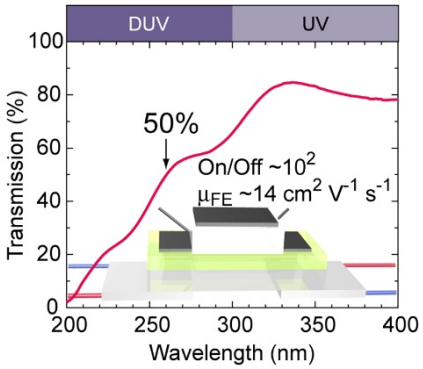

Supporting Information

Fabrication and Operating Mechanism of Deep-UV Transparent Semiconducting $SrSnO_3$-based Thin Film Transistor

Mian Wei, Lizhikun Gong, Dou-dou Liang, Hai Jun Cho, and Hiromichi Ohta**

M. Wei, L. Gong, Prof. H.J. Cho, Prof. H. Ohta
Graduate School of Information Science and Technology, Hokkaido University, N14W9, Kita, Sapporo 060−0814, Japan

D. Liang
The Beijing Municipal Key Laboratory of New Energy Materials and Technologies, School of Materials Science and Engineering, University of Science and Technology Beijing, Beijing 100083, China

D. Liang, Prof. H.J. Cho, Prof. H. Ohta
Research Institute for Electronic Science, Hokkaido University, N20W10, Kita, Sapporo 001−0020, Japan
E-mail: joon@es.hokudai.ac.jp, hiromichi.ohta@es.hokudai.ac.jp

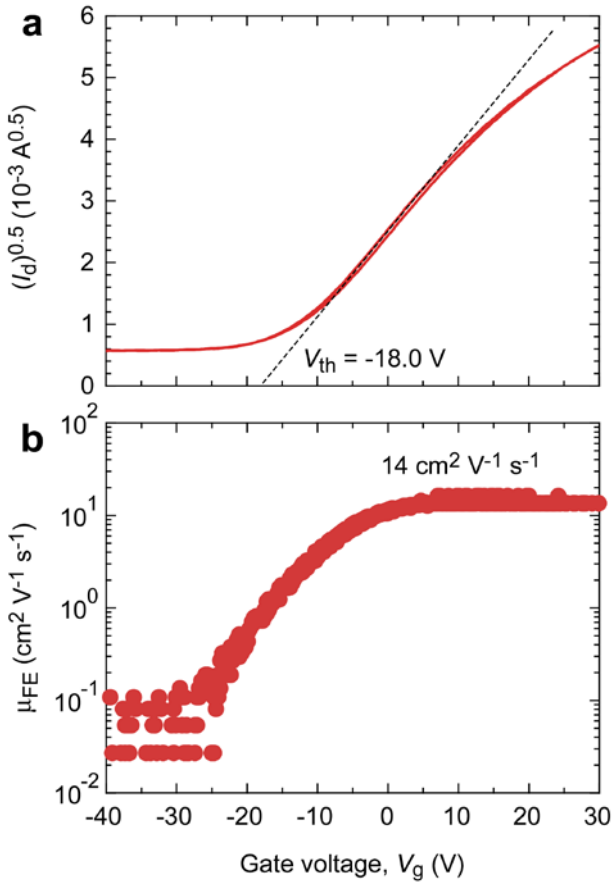

Figure S1. Detailed transistor characteristics of the $SrSnO_3$-based TFT. (a) $I_d^{0.5}$–V_g plot. The threshold voltage (V_{th}) is −18.0 V. (b) V_g dependence of the field effect mobility (μ_{FE}). μ_{FE} increases with V_g and reaches ~14 cm^2 V^{-1} s^{-1}.

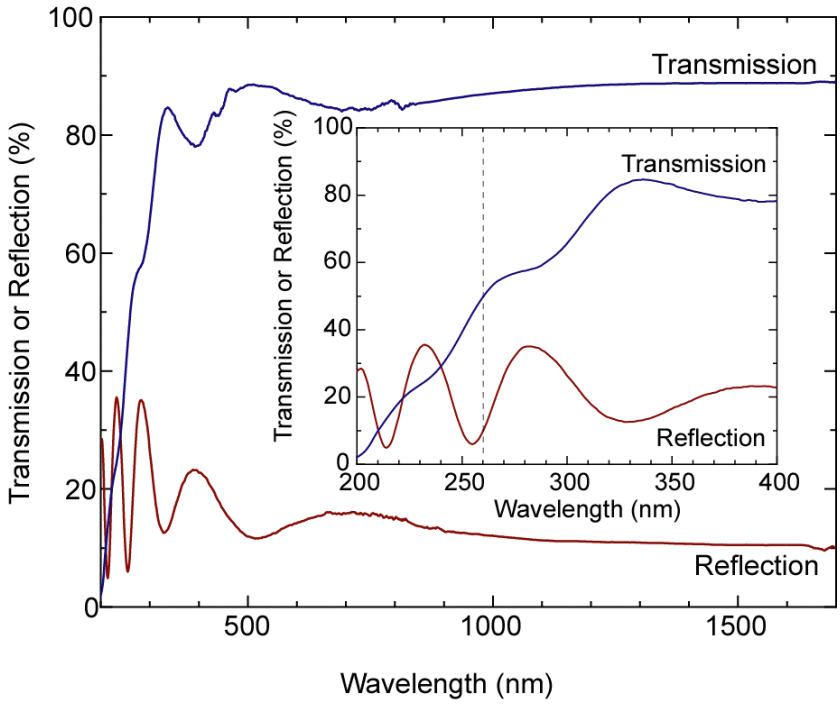

Figure S2. Optical transmission and reflection spectra of the multilayer of a-C12A7 film (300 nm) / La-doped $SrSnO_3$ film (23 nm) / (001) MgO substrate (0.5 mm). The optical transmission at 260 nm in wavelength is greater than 50%.

Table S1. **Electrical properties of La-doped $SrSnO_3$ ($La_xSr_{1-x}SnO_3$, x = 0.02, 0.03, and 0.05) films measured at room temperature.** We fabricated several $La_xSr_{1-x}SnO_3$ (x = 0.05, 0.03 and 0.02) epitaxial films on (001) $SrTiO_3$ single crystal. The electrical conductivity (σ), carrier concentration (n), and Hall mobility (μ_{Hall}) of the films were measured using the conventional dc four-probe method with van der Pauw electrode geometry at room temperature. The thermopower (S) was acquired from the thermos-electromotive force (ΔV) generated by a temperature difference (ΔT) of ~4 K across the film using two Peltier devices. The temperatures at each end of the films were simultaneously measured with two thermocouples, and the S-values were calculated from the slope of the $\Delta T-\Delta V$ plots (correlation coefficient: > 0.9999).

x in $(La_xSr_{1-x})SnO_3$	t (nm)	σ (S cm^{-1})	n ($\times 10^{20}$ cm^{-3})	μ_{Hall} (cm^2 V^{-1} s^{-1})	$-S$ (μV K^{-1})	m^* (m_e)
0.02	75.6	216	1.14	11.8	62	0.25
0.02	150	1242	2.24	34.6	45	0.28
0.03	91.8	190	1.12	10.6	66	0.26
0.03	135	612	1.4	27.3	48	0.22
0.03	58.3	554	1.08	32.0	55	0.21
0.03	124	1928	2.22	54.2	35	0.21
0.05	111	1134	1.73	40.9	48	0.25